International Symposium
On Turbulence and Shear Flow
Phenomena (TSFP-8)
August 28 - 30, 2013 Poitiers, France

NUMERICAL INVESTIGATION OF THE LAMINAR-TURBULENT TRANSITION IN A M=4.6 FLAT-PLATE BOUNDARY LAYER FORCED BY WALL INJECTION

E. Orlik
ICARE-CNRS
1C avenue de la Recherche Scientifique,
F-45071 Orléans cedex2, France
orlik@cnrs-orleans.fr

I. Fedioun
ICARE-CNRS
1C avenue de la Recherche Scientifique,
F-45071 Orléans cedex2, France
ivan.fedioun@cnrs-orleans.fr

N. Lardjane
CEA-DAM-DIF
F-91297 Arpajon, France
nicolas.lardjane@cea.fr

ABSTRACT

The laminar-turbulent transition of a Mach 4.6 flat-plate boundary layer forced by a wall under-expanded jet is investigated using Implicit Large Eddy Simulation based on a 5th order WENO scheme. Two free-stream unit length Reynolds numbers, 6 and 16 million, are considered. The effects of injection pressure and temperature on the structure and the stability of the near-injection flow are investigated. Downstream breakdown to turbulence is analyzed through Q-criterion visualization, mean velocity profiles and wall parameters. Results show that a low-pressure injection is sufficient for effective tripping, and that a cold injection is more efficient to promote transition.

INTRODUCTION

This study is conducted in the framework of airbreathing hypersonic flight, for which the control of the laminar-turbulent boundary layer (BL) transition is of primary importance. A turbulent boundary layer is mandatory to withstand the pressure gradients without separation, before being swallowed by the air inlet of the scramjet engine. Since natural transition at hypersonic flight conditions is very unlikely, passive or active devices must be used to insure transition. Passive devices may be isolated or distributed roughness, as investigated experimentally during the Hyper-X program by Berry *et al.* (2001). Such passive roughness are designed for a limited range of flight parameters and may not be efficient away from the design point. They may also trigger transition when a laminar BL is preferred, during booster acceleration for instance. The mechanisms associated with roughness-induced transition are still not fully understood (Schneider (2008)), though they are known to be relevant to the transient-growth theory as shown by Reshotko & Tumin (2004). Active devices, like wall injection, have received less attention and the literature on the subject is scarce. Active devices have obvious advantages over passive ones. They can be turned on or off on demand, with adjustable intensity to match any flight conditions. The major drawbacks are the needs to drill holes in the structure and to store high-pressure gas for injection. Asma *et al.* (2012) have studied experimentally the flow topology around tree- dimensional obstacles, and gas or liquid injection, and they have found many similarities in the flow structure, like the upstream separation zone, the presence of bow shock and the vortical structure downstream. Laminar-turbulent transition forced by wall injection has been studied experimentally by the Hyper-X transition team (Berry *et al.* (2004); Bathel *et al.* (2008)). These authors found that under-expanded jets may be very efficient, their effectiveness depending on the pressure ratio. The effect of CO_2 or Argon injection on transition in high enthalpy flows has been studied by Jewell *et al.* (2012). This work was aimed to delay transition, using the ability of CO_2 to damp the second (acoustic) Mack mode which is dominant at high Mach number. It was found that the transition location depends on the injection mass flow rate: a low value delays transition while a high mass flow rate promotes transition.

Under-expanded jets in supersonic crossflow (JISC) have been extensively studied for turbulent fuel-air mixing in scramjets, both experimentally by Schetz *et al.* (1967); Santiago & Dutton (1997), and numerically using either Reynolds averaged simulations (RANS) (Viti *et al.* (2009)), large-eddy simulations (LES) (Kawai & Lele (2010)) or implicit large-eddy simulations (ILES) (Chai & Mahesh (2010, 2011); Rana *et al.* (2011)), and the physics of this flow is well understood. However, JISC for BL tripping have received less attention, although the idea of tripping a BL with discrete jets goes back at least forty years ago (Stone & Cary (1972)). Nowadays, the development of higher-order numerical methods and the increase in computational power make the numerical investigation of hypersonic BL transition possible. Direct numerical simulation (DNS) is the very expensive cutting-edge research tool (Zhong & Wang (2012)). An example of such DNS is the work of Bernardini *et al.* (2012) who investigated the BL transition downstream an isolated cubic roughness, using about 20 million grid points in a quite limited computational

Table 1. Free stream conditions.

Flow	T_∞ (K)	P_∞ (Pa)	U_∞ (m/s)	$(\rho U)_\infty$ (kg/m^2.s)	Re_∞ (10^6/m)
hot	340	6844	1700	119	6
cold	76	2455	804	90.5	16

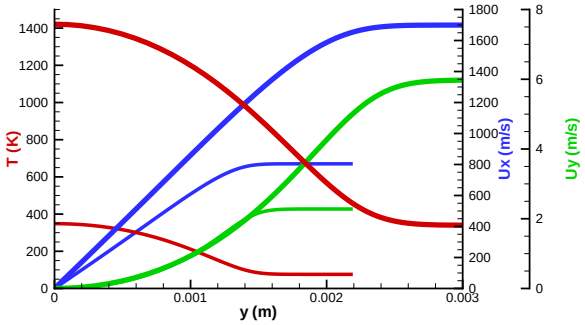

Figure 1. Levy-Lees boundary layer inlet profiles.

domain. Other examples are given by Iyer *et al.* (2010) and by Muppidi & Mahesh (2012) for the transition downstream an isolated bump or distributed roughness at Mach number 2.9, but again, very few (if any) numerical studies of transition induced by JISC can be found in the literature.

This paper investigates the transition downstream of an isolated sonic wall injection into a supersonic boundary layer, using the ILES technique based on a 5th order WENO scheme. Descriptions of the WENO method and ILES procedure can be found in Shu (1997, 2009) and Karaca *et al.* (2012). Although the grid is not fine enough to observe near-wall fully developed coherent structures in the final stage of transition, some clear trends can be observed regarding the tripping efficiency in each case.

COMPUTATIONAL SETUP

For the purpose of the present study, an academic M_∞=4.6 flat-plate configuration is considered. The self-similar Levy-Lees (LL) laminar solution serves as inlet condition for the ILES-WENO simulation. Two free stream values are considered, whose parameters are listed in table 1. The "hot" flow is typical of flight or hot-shot wind tunnel conditions, whereas the "cold" flow may represent a blow-down wind tunnel that operates at room or slightly heated stagnation temperature. Figure 1 displays the inlet velocity and temperature LL profiles, taken at $x_{LL} = 0.25$ m and $x_{LL} = 0.20$ m for the hot and cold flow, respectively. Figure 2 (cold flow) shows that the WENO code keeps the LL solution far downstream.

A sonic top-hat injection velocity profile is applied 0.12 m downstream from the inlet through a hole of diameter 1 mm. At the injection location, the BL thickness is $\delta \approx 3$ mm for the hot flow and $\delta \approx 2$ mm for the cold flow. Injection parameters are listed in table 2. The last column indicates the wall temperature, hence a cold or hot flow. Static and total injection temperatures are respectively 300 K and 360 K for cases (a), (c), (d) and (f). In cases (b) and (e), the static and total temperatures are chosen to keep the same temperature ratio T_{inj}/T_{wall} as in cases (a) and (d). In cases (c) and (f), the jet is cold compared to the incoming flow. The pressure ratio PR=$P_{tot,inj}/P_\infty$ is either 15.4 or 77.

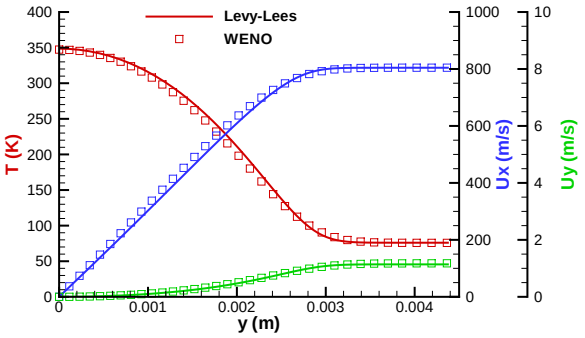

Figure 2. Comparison of WENO (Navier-Stokes) and Levy-Lees solutions at $x_{LL} = 0.80$ m.

Table 2. Injection parameters.

case	PR	$P_{tot,inj}$ (kPa)	P_{inj} (kPa)	$T_{tot,inj}$ (K)	T_{inj} (K)	$(\rho U)_{inj}$ (kg/m^2.s)	T_{wall} (K)
(a)	15.4	37.82	20	360	300	80	340
(b)	15.4	105.4	56	1620	1400	101	1400
(c)	15.4	105.4	56	360	300	225	1400
(d)	77.0	189.1	100	360	300	402	340
(e)	77.0	527.2	278	1620	1400	495	1400
(f)	77.0	527.2	278	360	300	1119	1400

The computational domain shown in figure 3 is a rectangular parallelepiped whose dimensions are $L_x = 0.985$ m, $L_y = 0.025$ m, $L_z = 0.1$ m. The size of the cartesian grid is $N_x \times N_y \times N_z = 512 \times 192 \times 135$ ($\approx 13 \times 10^6$ grid points). It is clustered close to the wall and around the injection hole, with smallest grid cells $\Delta x_{min} = \Delta z_{min} = 0.16$ mm, and $\Delta y_{min} = 0.038$ mm. There are only 6 grid points in the hole diameter. At the end of the computational domain, the mesh, stretched in the x longitudinal direction, is quite coarse for a well resolved ILES but fine enough in the z transverse direction, and the viscous sublayer is properly resolved.

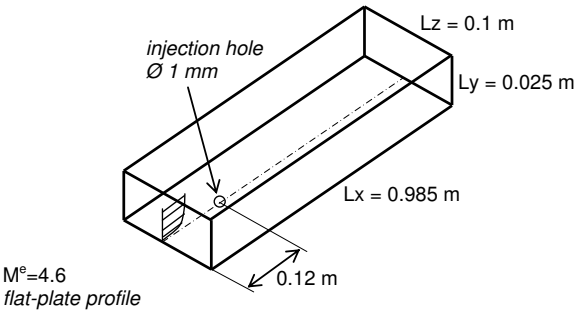

Figure 3. Computational domain.

NEAR-INJECTION FLOW STRUCTURE

Transition occurrence or not is a direct consequence of the flow structure in the jet region. Hence, particular attention has been paid to its proper resolution and to the understanding of how it is influenced by the injection parameters. The well known flow structure (Viti *et al.* (2009))

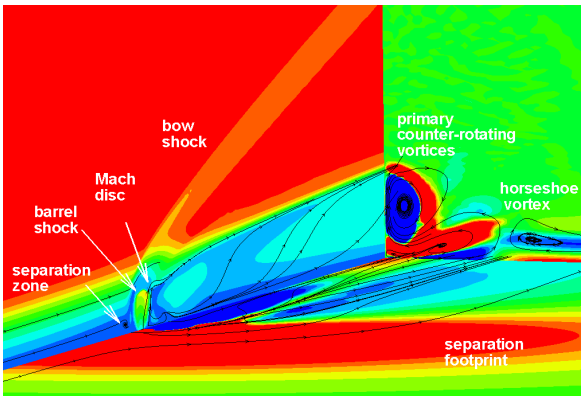

Figure 4. Contour of Mach number in the symmetry plane, wall pressure, x-vorticity in the $x = 0.15$ m plane, case (b).

is shown in figure 4 for case (b). One can clearly see the main bow shock due to the jet, the barrel shape of the under-expanded jet ending with a Mach disk, the separation zone ahead of the jet, the footprint of near wall horseshoe vortices (HSV) and the primary counter rotating longitudinal vortices (CRV).

The jet penetration, defined as the ratio h/δ of the height of the Mach disk to the incoming BL thickness, is an important parameter for the tripping efficiency, like the ratio k/δ in the case of isolated solid trips of height k. Figure 5 displays the jet penetration for all cases. It is typically in the range of effectiveness, or above, for isolated solid trips (Schneider (2008); Alba *et al.* (2008)).

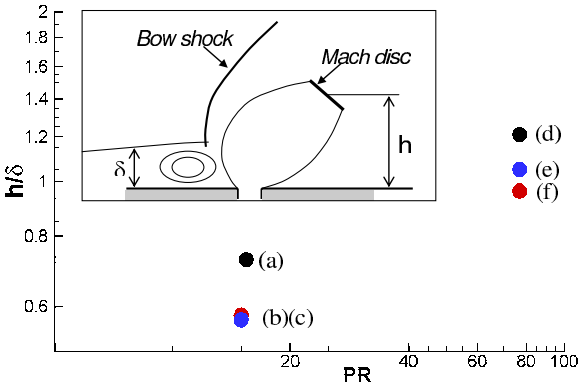

Figure 5. Ratio of the height of the Mach disc to the BL thickness versus PR. Black: cases (a) and (d), blue: cases (b) and (e), red: cases (c) and (f).

More information about flow structure can be obtained using the Q- criterion (Dubief & Delcayre (2000)). Figure 6 displays the same instantaneous Q- isovalue colored by the x vorticity component for cases (a) and (d) in the injection region. In case (d) where the Mach disc is above the BL, the CRV start to oscillate in the free stream at about 50 kHz.

TRANSITION RESULTS

Turbulence is a chaotic motion of the flow around mean values, hence the occurrence of fluctuations in the flow is

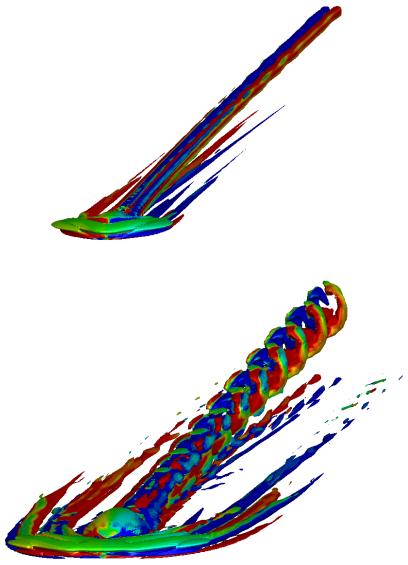

Figure 6. Q-criterion colored by x vorticity component, top: case (a), bottom: case (d).

the first indicator that it became turbulent. As a consequence, global or average flow characteristics are dramatically changed. Hence, the detection of the position of the laminar-turbulent transition is mainly based on the measurements of two kinds of changes in the BL: (i) unsteady characteristics of the flow due to turbulent fluctuations, (ii) mean wall characteristics like temperature, heat flux, skin friction.

In the review work of Lowson (1968), it is shown that the wall pressure pulsation normalized by the wall shear stress τ_w is a suitable parameter for turbulent supersonic boundary layers:

$$\frac{P_{RMS}}{\tau_w} \in [2,4] \tag{1}$$

Also, the level of pressure fluctuations can be empirically related to the free stream pressure and Mach number:

$$\frac{P_{RMS}}{P_\infty} \approx \frac{0.0042}{\mathrm{M}_\infty^{-2} + 0.14} = 0.022 \tag{2}$$

The adiabatic wall temperature is defined, under the assumption of constant C_p, by

$$\frac{T_{w_{ad}}}{T_\infty} = 1 + r\left(\frac{\gamma-1}{2}\right)\mathrm{M}_\infty^2 \tag{3}$$

where the recovery factor r is $\sqrt{Pr}$ for a laminar and $\sqrt[3]{Pr}$ for a turbulent BL. These values for air are 0.83 and 0.9 correspondingly. The ratio $T_{w_{turb}}/T_{w_{lam}}$ is then expected about 1.045. Maps of instantaneous wall pressure, *RMS* pressure, and mean temperature are shown in figure 7. All data indicate the presence of a turbulent near-wall flow downstream the injection port. Moreover, computed values are in accordance with theoretical and empirical predictions, and prove the quality of ILES computations.

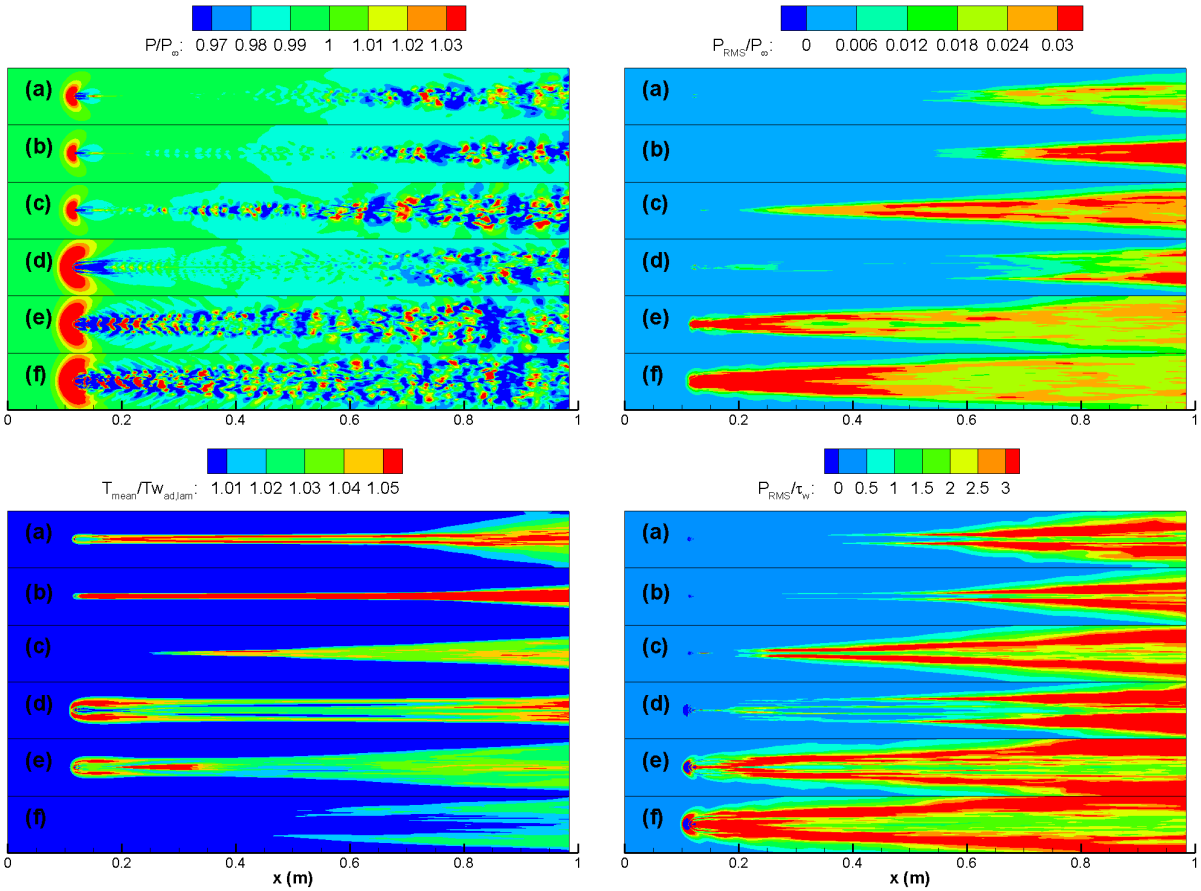

Figure 7. Clockwise from top-left: Instantaneous wall pressure, *RMS* wall pressure, eq. (1), mean wall temperature.

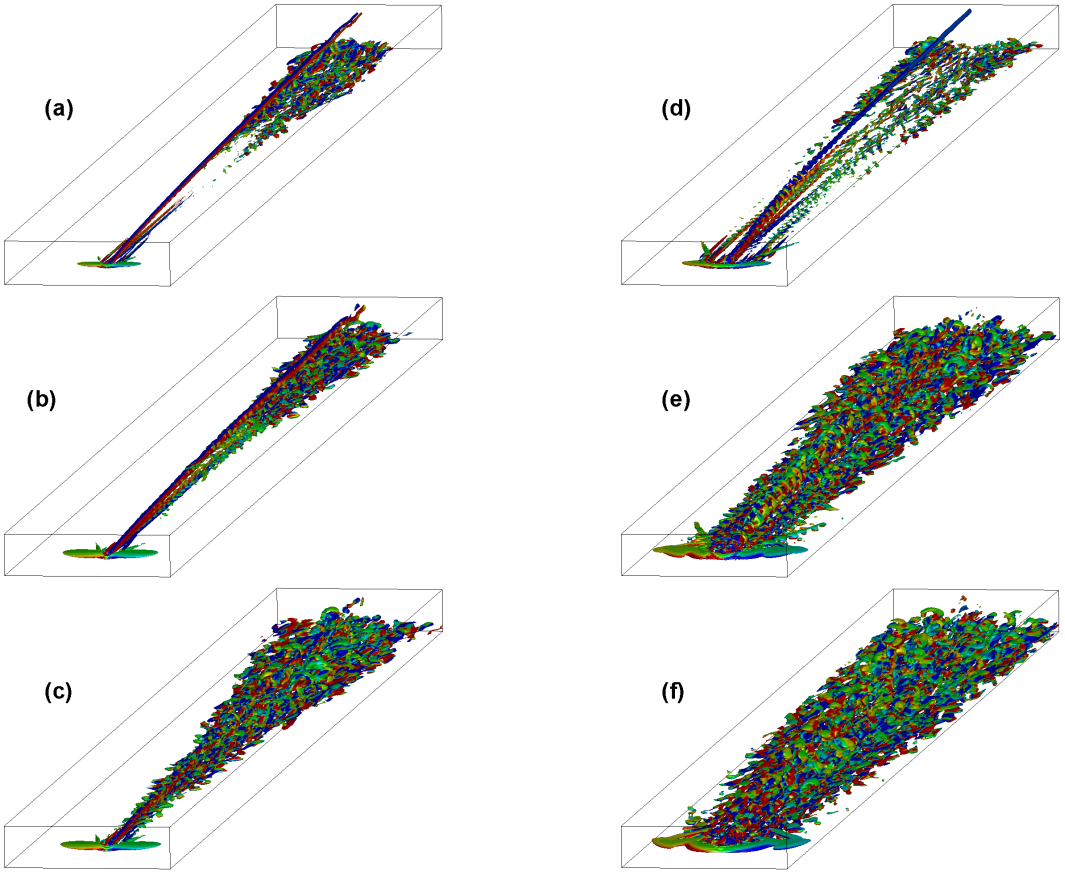

Figure 8. *Q*-criterion colored by *x* vorticity component. Cases (a) to (f) : see table 2.

In LES or DNS results, the occurrence of transition can be detected qualitatively from coherent structures observed both in the near-injection region and in the downstream development of the BL. Figure 8 displays, with the same scale, the same isovalue of the Q-criterion colored by the x vorticity component for cases (a) to (f). Visual analysis from figures 7 and 8 reveals that :

- In cases (a), (b) and (c), for which the Mach disc is below the BL edge ($h/\delta \leq 1$), the CRV are stable. Transition occurs in the wake of near-wall HSV that destabilize at $x \approx 0.6$ m for case (a) and (b). In case (c), transition occurs significantly upstream, although the height of Mach disk is almost the same. The injected mass flow rate is however higher than in cases (a) and (b), because of the cold injection condition (see table 2). Relevant empirical criteria for roughness-induced transition are based on the trip edge Reynolds number Re_{kk}. By analogy, one could investigate the influence of the Reynolds number at the Mach disk height, or the Reynolds number based on the jet diameter. This will be the subject of further investigations.
- At higher PR, cases (d), (e) and (f), the Mach disc is just at, or above, the BL edge, and CRV start to oscillate in the free stream. In case (d) the instantaneous wall pressure reveals these oscillations up to $x \approx 0.3$ m (see also figure 6). The structure of HSV is affected and transition is delayed to $x \approx 0.7$ m.
- For cases (e) and (f), CRV enter a self-sustained harmonic motion that drives the whole flow field to transition downstream. The instantaneous wall pressure is deeply affected up to $x \approx 0.3$ m, but this is not the footprint of transition. In case (f), the self-sustained motion has a lower frequency compared to cases (d) or (e).
- In case (f), the cooling of the wall by cold injected air is observed in the temperature map of figure 7. Hence temperature measurement would not be an efficient experimental technique to detect the laminar-turbulent transition.

Time-averaged velocity profiles can be plotted in semi-log coordinates using the van Driest (1951) transform

$$U_{vd} = \frac{U_\infty}{A}\left\{\sin^{-1}\left[\frac{2A^2U/U_\infty - B}{\sqrt{B^2+4A^2}}\right] + \sin^{-1}\left[\frac{B}{\sqrt{B^2+4A^2}}\right]\right\} \quad (4)$$

$$A = \sqrt{\frac{\gamma-1}{2}\mathrm{Pr}_t \mathrm{M}_\infty^2 \frac{T_\infty}{T_w}} \quad ; \quad B = \left[1 + \mathrm{Pr}_t^{1/2}\frac{\gamma-1}{2}\mathrm{M}_\infty^2\right]\frac{T_\infty}{T_w} - 1$$

for comparison with the incompressible law of the wall in inner variables $u^+ = U_{vd}/U_\tau = f(y^+)$. Velocity profiles are analyzed at the far downstream location x=0.95 m for different transverse z positions. Transition to turbulence is indicated by their departure from a linear behavior $u^+ \approx y^+$ outside the viscous sublayer ($y^+ \gtrsim 10$). It is not expected that a tripped BL in the transition stage match accurately these fully developed turbulent flat-plate correlations, neither it exhibits a logarithmic profile. They are anyway useful indicators. We restrict the analysis of velocity profiles to cases (c) and (f), the most efficient ones for transition at low and high PR, respectively. Velocity profiles in figure 9 (left) clearly show that the BL for case (c) is laminar at $z = 0.03$ m. A departure from a laminar behavior is observed at $z = 0.02$ m. At $z = 0.01$ m and in the symmetry plane, velocity profiles are typical of a turbulent BL although, as in Iyer *et al.* (2010), the log law is not well established. In case (f) with high PR, velocity profiles (right part of figure 9) indicate that transition spreads spanwise.

The wall shear stress normalized by the local, laminar, non-tripped value, is plotted in figure 10 along x in different z planes for all cases (left: low PR cases (a), (b) and (c), right: high PR cases (d), (e) and (f). Transition creates a rise from unity, but high values are also observed in the symmetry plane in the wake of the jet in any case. In the low PR case (left part of figure 10), transition is apparent in the $z = 0.01$ m and $z = 0.02$ m planes, and confirms case (c) to be the most efficient. Results for the high PR case (right part of figure 10) are more confused. Case (d) stays laminar in the $z = 0.02$ m plane, but all other curves show a more or less rapid increase in the wall shear stress downstream of the injection port.

CONCLUSIONS AND PERSPECTIVES

From these numerical experiments (and from other cases of injection not presented here) of a supersonic M=4.6 boundary layer tripped by under-expanded JISC, some conclusions about the transition process can be proposed.

At low PR and same jet temperature as the wall temperature, transition appears to be mainly due to the inviscid destabilization of near-wall HSV coming from the separation region ahead of the injection port. As the pressure ratio is increased, the Mach disc, hence the initial development of CRV which were first below the incoming BL thickness, move into the free stream. Once the Mach disc is in the free stream, CRV enter a self-sustained oscillating motion that impacts the structure of HSV and delay transition (case (a) $\rightarrow$ (d)). However, in some cases like (e), the flow is so much perturbed by the CRV oscillations that transition occurs by forcing from the free stream.

The jet temperature is also an important parameter. While wall cooling stabilizes the first Tollmien-Schlichting mode, a cold injection, hence a high mass flow rate, is more destabilizing here. In-depth theoretical analysis of instability mechanisms, in the framework of the transient growth and optimal perturbation theories will help, together with additional simulations and experiments, understanding fully the breakdown to turbulence by JISC.

ACKNOWLEDGEMENTS

This work was granted access to the HPC resources of IDRIS under the allocation 2012-020913 made by GENCI (Grand Equipement National de Calcul Intensif).

REFERENCES

Alba, C.R., Johnson, H.B., Bartkowicz, M.D. & Candler, G.V. 2008 Boundary-layer stability calculations for the hifire-1 transition experiment. *Journal of Spacecraft and Rockets* **45** (6), 1125–1133.

Asma, C.O., Tirtey, S. & Schloegel, F. 2012 Flow topology around gas, liquid, and three-dimensional obstacles in hypersonic flow. *AIAA Journal* **50** (1), 1100–108.

Bathel, B.F., Danehy, P.M., Inman, J.A., Alderfer, D.W. & Berry, S.A. 2008 Plif visualization of active control of hypersonic boundary layers using blowing. AIAA paper 2008-4266.

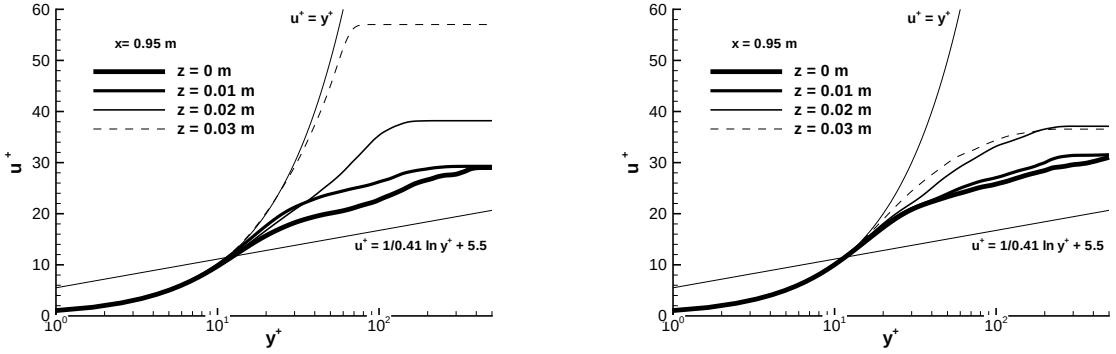

Figure 9. Van Driest velocity profiles, x=0.95 m. Left: case (c), low PR. Right: case (f), high PR.

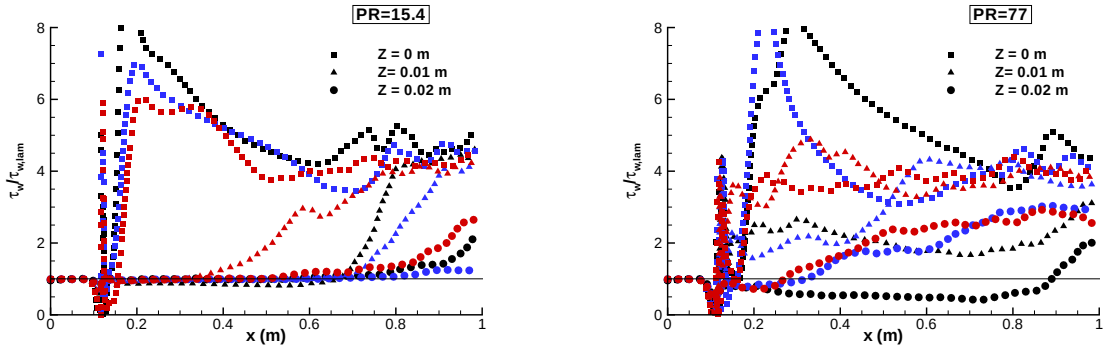

Figure 10. Normalized wall shear stress in different z planes. Left: low PR, right: high PR. Black: cases (a) and (d), blue: cases (b) and (e), red: cases (c) and (f).

Bernardini, M., Pirozzoli, S. & Orlandi, P. 2012 Compressibility effects on roughness-induced boundary layer transition. *International Journal of Heat and Fluid Flow* **35**, 45–51.

Berry, S.A., Auslender, A.H., Dilley, A.D. & Calleja, J.F. 2001 Hypersonic boundary-layer trip development for hyper-x. *Journal of Spacecraft and Rockets* **38**, 853–864.

Berry, S.A., Nowak, R.J. & Horvath, T.J. 2004 Boundary layer control for hypersonic airbreathing vehicles. AIAA paper 2004-2246.

Chai, X. & Mahesh, K. 2010 Simulations of high speed turbulent jets in crossflow. AIAA paper 2010-4603.

Chai, X. & Mahesh, K. 2011 Simulations of high speed turbulent jets in crossflow. AIAA paper 2011-650.

van Driest, E. 1951 Turbulent boundary layer in compressible fluid. *Journal of the Aeronautical Sciences* **18** (3), 145–160.

Dubief, Y. & Delcayre, F. 2000 On coherent-vortex identification in turbulence. *Journal of Turbulence* **1** (11), 1–22.

Iyer, P.S., Muppidi, S. & Mahesh, K. 2010 Transition of hypersonic flow past flat plate with roughness elements. AIAA paper 2010-5015.

Jewell, J.S., Leyva, I.A., Parziale, N.J. & Shepherd, J.E. 2012 Effect of gas injection on transition in hypervelocity boundary layers. pp. 735–740. San Diego, CA, 28th International Symposium on Shock Waves.

Karaca, M., Lardjane, N. & Fedioun, I. 2012 Implicit large eddy simulation of high-speed non-reacting and reacting air/h_2 jets with a 5th order weno scheme. *Computers & Fluids* **62**, 25–44.

Kawai, S. & Lele, S.K. 2010 Large-eddy simulation of jet mixing in supersonic crossflows. *AIAA Journal* **21** (9), 2063–2083.

Lowson, M.V. 1968 Predictions of boundary layer pressure fluctuations. TR AFFDL-TR-67-167.

Muppidi, S. & Mahesh, K. 2012 DNS of roughness-induced transition in supersonic boundary layers. *Journal of Fluid Mechanics* **693**, 28–56.

Rana, Z.A., Thornber, B. & Drikakis, D. 2011 Transverse jet injection into a supersonic turbulent cross-flow. *Physics of Fluids* **23** (9), 2063–2083, 046103.

Reshotko, E. & Tumin, A. 2004 Role of transient growth in roughness-induced transition. *AIAA J.* **42**, 766–771.

Santiago, J.G. & Dutton, J.C. 1997 Velocity measurements of a jet injected into a supersonic crossflow. *Journal of Propulsion and Power* **13**, 264–273.

Schetz, J.A., Hawkins, P.F. & Lehman, H. 1967 Structure of highly underexpanded transverse jets in a supersonic stream. *AIAA Journal* **5**, 882–884.

Schneider, S.P. 2008 Effects of roughness on hypersonic boundary-layer transition. *Journal of Spacecraft and Rockets* **45**, 193–209.

Shu, C.W. 1997 Essentially non-oscillatory and weighted essentially non-oscillatory schemes for hyperbolic conservation laws. NASA/CR-97-206253 ICASE 97-65. Langley Research Center.

Shu, C.W. 2009 High order weighted essentially non-oscillatory schemes for convection dominated problems. *SIAM Review* **45** (1), 82–126.

Stone, D.R. & Cary, A.M. 1972 Discrete sonic jets used as boundary-layer trips at mach numbers of 6 and 8.5. NASA TN D-6802.

Viti, V., Neel, R. & Schetz, J.A. 2009 Detailed flow physics of the supersonic jet interaction flow field. *Physics of Fluids* **21**, 264–273.

Zhong, X. & Wang, X. 2012 Direct numerical simulation on the receptivity, instability, and transition of hypersonic boundary layers. *Annu. Rev. Fluid Mech.* **44**, 527–561.